Chemical Geology 715 (2026) 123486

Contents lists available at ScienceDirect

Chemical Geology

journal homepage: www.elsevier.com/locate/chemgeo

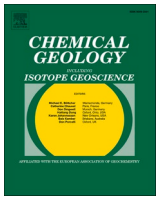

Bedrock testing of zircon annealing for detrital provenance studies: Raman and U-Pb analysis in the Adamello batholith (Southern Alps, Italy)

Alberto Resentini [a], Marco G. Malusà [a,*], Silvia Favaro [a], Michele Longhi [a], Massimo Tiepolo [b], Igor M. Villa [a,c], Stefano Zanchetta [a]

[a] Department of Earth and Environmental Sciences, University of Milano-Bicocca, 20126 Milan, Italy
[b] Department of Earth Sciences "A. Desio", University of Milano, Via Botticelli 23, 20133 Milan, Italy
[c] Institute of Geological Sciences, University of Bern, Switzerland

ARTICLE INFO

Editor: Christian France-Lanord

Keywords:
Zircon U-Pb dating
Raman analysis
α-damage annealing
Detrital geochronology
Provenance discrimination
European Alps

ABSTRACT

We present a new conceptual model for the interpretation of bedrock and detrital zircon data based on a comparison between theoretical α-damage inferred from U-Pb data and actual α-damage measured by Raman analysis. The model is tested in the Cenozoic Adamello composite batholith in the Southern Alps (Italy), a natural laboratory where the progressive emplacement of successive magmatic bodies has thermally affected both the metamorphic country rocks and the previously emplaced igneous rocks under well-constrained geological conditions. Bedrock samples were collected along a traverse that spans the contact between plutons of different ages and their country rocks. We found that: (i) zircon rims from the Adamello batholith invariably show a complex, but consistent annealing history after crystallization, as induced by subsequent intrusion of younger plutonic bodies; (ii) zircon cores record damage accumulation starting from the age of rim crystallization; (iii) the severity of annealing in country rock zircons correlates with distance from the nearby plutons. Results on bedrock zircon are then exported to a synthetic detrital zircon population to test how the impact of reheating can be detected in detritus. We found that the application of our model allows increasing the resolution of provenance discrimination, providing a level of information approaching the evolution inferred from bedrock data. We conclude that an approach to detrital zircon geochronology complementing detrital U-Pb ages with Raman spectroscopy could open new venues in sediment provenance analysis and could be proficiently used to improve the identification of clastic detritus sources.

1. Introduction

Zircon ($ZrSiO_4$) U-Pb dating is a fundamental tool to assess rock formation age and understand Earth evolution (Harley and Kelly, 2007; Voice et al., 2011; Schoene et al., 2019). It is based on the natural incorporation of U and Th in the zircon structure during crystallization and on the subsequent formation of daughter isotopes produced by U and Th decay to eventually form stable Pb (Jaffey et al., 1971). As an effect of the multiple α and β decay events, the crystal structure of the host zircon is progressively damaged. In old and U-rich grains the damage can accumulate up to a point where the crystalline zircon reaches an amorphous state (metamict zircon, Ewing et al., 1987). Damage can be quantified via Raman spectroscopy based on the position and width of the SiO_4 bands, as they shift to lower positions and get progressively broader as damage is accumulated (Nasdala et al., 1998, 2001). Damage can be annealed, as the amorphized portions of the lattice can reacquire their crystalline structure with heating (Zhang et al., 2000; Geisler, 2002). This feature has been explored as a new potential thermochronological method (Pidgeon et al., 1998; Härtel et al., 2021a) to obtain a multi-faceted, overall better constrained characterization of the geological history of zircon crystals via Raman spectroscopy, a non-destructive technique that allows the evaluation of the lattice damage and preserves the zircon grains for other complementary analyses.

Previous studies have focussed mainly on the calibration of a zircon-Raman geochronometer based on the analysis of "standard" crystals showing a well-constrained geologic history of continuous damage accumulation and little-to-no annealing after crystallization (Härtel et al., 2021a, 2024; Fan et al., 2023; Su et al., 2023). By contrast, zircon crystals affected by annealing events have received less attention (e.g.,

* Corresponding author.
E-mail address: marco.malusa@unimib.it (M.G. Malusà).

https://doi.org/10.1016/j.chemgeo.2026.123486
Received 5 February 2026; Received in revised form 11 May 2026; Accepted 12 May 2026
Available online 13 May 2026

Resentini et al., 2020; Härtel et al., 2022; Zhang et al., 2026), as the partial loss of accumulated damage makes the interpretation of Raman results more challenging. However, due to its high resistance and durability, zircon can usually survive multiple sedimentary and metamorphic cycles (Velbel, 1999; Malusà et al., 2013; Malusà and Garzanti, 2019), and zircons that have undergone reheating and annealing since their crystallization are by far dominant in the sedimentary record.

In this study, we present a new conceptual model that combines U-Pb dating and Raman analysis of bedrock zircon grains to explore how the annealing of radiation damage can be used to better constrain the geologic evolution of detrital zircon grains and reconstruct the geological landscape of the distant past. We use the Adamello composite batholith in the European Alps as a natural laboratory, as it is an area where the successive emplacement of radiometrically dated magmatic bodies has thermally affected both the metamorphic country rocks and the previously emplaced igneous rocks under controlled geological conditions (Brack. et al., 2008; Ji et al., 2019). Our results on bedrock zircon crystals are then exported to synthetic detrital zircon populations, to demonstrate how the impact of reheating can be detected in natural detrital zircon datasets and can be used to improve sediment provenance analysis in other study areas.

2. Conceptual model

2.1. Quantification of zircon α-damage

Knowing the age and actinide content of a zircon crystal, the accumulated radiation damage can be approximated as the number of α-decay events (N_α) of that crystal. This number can be estimated according to the formula proposed by Murakami et al. (1991) after Holland and Gottfried (1955):

$$N_\alpha = 8\,N_{238-U}\,[\exp(\lambda_{238}\,t)-1] + 7\,N_{235-U}\,[\exp(\lambda_{235}\,t)-1] + 6\,N_{232-Th}\,[\exp(\lambda_{232}\,t)-1] \quad (1)$$

where: N_α is expressed in *α events/g*; $N_{238\text{-}U}$, $N_{235\text{-}U}$ and $N_{232\text{-}Th}$ are the present numbers of ^{238}U, ^{235}U, and ^{232}Th in *atoms/g*; λ_{238}, λ_{235}, and λ_{232} are their respective decay constant in $years^{-1}$; and t is the crystallization age of the zircon (Murakami et al., 1991).

Alpha-damage can be estimated also by Raman analysis, using the N_α-bandwidth calibration lines reported in Härtel et al. (2021a) for the 4 main SiO_4 Raman bands of zircon related to External Rotation (ER) at ~356 cm^{-1}, symmetric stretching (ν_1) at ~975 cm^{-1}, symmetric bending (ν_2) at ~439 cm^{-1}, and anti-symmetric stretching (ν_3) at ~1008 cm^{-1} (Dawson et al., 1971; Kolesov et al., 2001). Raman-estimated α-damage (here cumulatively referred to as RD_α or individually as $RD_{ER\alpha}$, $RD_{\nu1\alpha}$, $RD_{\nu2\alpha}$, $RD_{\nu3\alpha}$) represents the "actual" damage that is currently stored within the crystalline structure of the zircon and is thus the combined result of damage accumulation and (partial) annealing. The general form for these calibration lines is:

$$\text{Raman estimated α-damage}\left(10^{16}\ \alpha\text{-events}\ g^{-1}\right) = (\Gamma - b)/a \quad (2)$$

where Γ is the measured full width at half maximum of the Raman band (in cm^{-1}), b is the Γ for zero-damage zircon (in cm^{-1}) and a represents the α-damage response (in $cm^{-1}/10^{16}\ \alpha\ events\ g^{-1}$). Values for a and b, as indicated in Härtel et al. (2021a) are reported below:

$$RD_{ER\alpha} = (\Gamma_{ER} - 4.04)/0.171 \quad (3)$$

$$RD_{\nu1\alpha} = (\Gamma_{\nu1} - 1.86)/0.107 \quad (4)$$

$$RD_{\nu2\alpha} = (\Gamma_{\nu2} - 5.16)/0.141 \quad (5)$$

$$RD_{\nu3\alpha} = (\Gamma_{\nu3} - 2.85)/0.111 \quad (6)$$

These calibration lines are derived from Γ values corresponding to different damages (N_α values) from zircon grains that experienced no annealing since crystallization and thus represent continuous accumulation. In zircon grains that did not experience annealing, RD_α values are close to N_α, whereas RD_α lower than N_α indicate annealing. Damage accumulation/annealing can be estimated from any of the four main Raman bands. However, the ER Raman band is the most sensitive to annealing (Härtel et al., 2021b; McKanna et al., 2023) and is thus the one considered in this work to reveal the zircon annealing history.

2.2. Damage accumulation and simplified annealing model

After zircon crystallization, damage starts to accumulate and Raman bandwidths increase following the continuous accumulation line (Fig. 1). If measured $RD_{ER\alpha}$ is lower than N_α, annealing necessarily occurred at some time during the zircon history, and the zircon Γ vs. N_α value plots to the right of the "complete accumulation" line that is defined by Eq. (2), as indicated in Fig. 1a. The accumulation of α-damage in the zircon structure over time can be modeled by applying formula (1) using varying *t* from crystallization age to today (dark blue line in – Fig. 1 b). This produces a set of values for α-events/g ranging from 0 (i.e. the damage accumulated at the time of crystallization) to N_α (i.e. the maximum damage accumulated since crystallization) calculated using formula (1). Each zircon is expected to accumulate damage at a rate that depends on its characteristic actinide content. Zircon grains richer in U and Th (Fig. 1b) will accumulate damage faster than zircon grains with lower U and Th (Fig. 1d). Similarly, it is possible to model the evolution of the Raman band widths for each damage value by applying formula (2) (dark blue line in Fig. 1c).

In cases where thermal overprint was strong enough to completely anneal any damage in the zircon crystalline structure, we can calculate the age of such an annealing event. Complete annealing, by definition, fully restores the crystalline structure in a zircon grain. After annealing, each zircon grain starts accumulating damage at its own characteristic rate, given by its U and Th content, until a damage equal to $RD_{ER\alpha}$ is reached (Fig. 1 b,d). The timing of such inferred complete annealing can be estimated by forward modelling the accumulated damage that each grain would display if annealing took place *t* Ma ago and damage started to accumulate since then. The modeled damages can be compared to the observed $RD_{ER\alpha}$, defining the most plausible age of complete annealing (time intercept of the dashed line in Fig. 1b,d). To account for uncertainties in data acquisition and the model itself, we consider as acceptable any age that allows to forward model $RD_{ER\alpha}$ achieving a ratio with measured $RD_{ER\alpha}$ in the interval between 0.9 and 1.1. In bedrock samples, the age of such a total annealing event should be roughly the same for any zircon crystal from the same rock. In that case, the modeled damage accumulated since annealing corresponds to the measured bandwidth in Fig. 1c.

2.3. Total vs partial annealing

The retrieved maximum age of the last annealing event (maximum age, total annealing in Fig. 1b-d) can be geologically meaningful, if it is concomitant with an independently known major magmatic or metamorphic event. If the inferred total annealing age is older than any known magmatic or metamorphic event in the study region, it is probable that the crystalline structure of the zircon crystals was only partially annealed. In that case, provided that the age of annealing can be deduced from the geological context, we can model the accumulation of damage since crystallization taking into account different degrees of damage recovery at the independently known time of annealing. Red lines in Fig. 1b,d illustrate this approach. The annealing is forward modeled as a fraction of the total damage accumulated since crystallization. For each zircon grain, the most likely degree of partial annealing can be estimated by requiring that the final modeled damage be equal to the measured $RD_{ER\alpha}$. When multiple annealing events are suspected, the same simple approach of Fig. 1 can be applied to subsequent annealing events, provided that the age of the annealing events is known and the

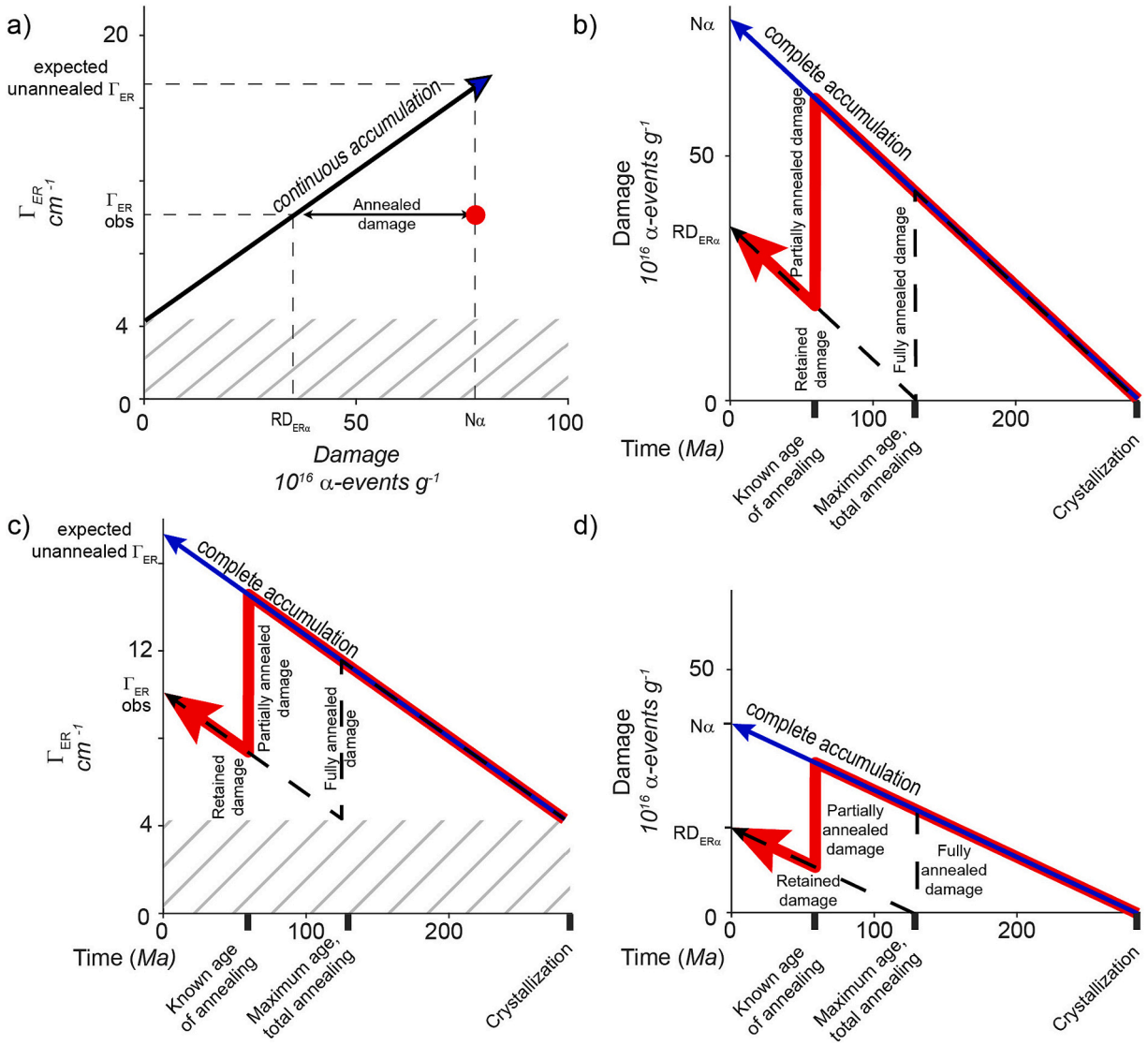

Fig. 1. Simplified model of damage accumulation and annealing for a zircon crystal. a: Γ_{ER} vs. damage. If the observed Γ_{ER} (Γ_{ER} obs) is lower than the expected unannealed Γ_{ER} corresponding to the damage accumulated since crystallization (N_α), i.e., the red dot does not lay along the continuous accumulation line (in black, Härtel et al., 2021a), the zircon grain underwent annealing. The difference between the maximum theoretical damage (N_α) and the damage measured with Raman spectroscopy ($RD_{ER\alpha}$) represents the amount of the annealed damage. $\Gamma_{ER} = 4.04$ is the lowest value for zero-damage zircon, values lower than 4.04 (hatched area) are thus impossible. b: damage accumulation since crystallization and potential annealing perturbations, following the red or the dashed black line, for the same annealed zircon grain depicted in panel (a). c: Raman ER-band broadening/narrowing as caused by damage accumulation/annealing for the same zircon grain depicted in panels (a) and (b). d: same as (b) for a U-Th-poor zircon grain (note the change in slope of the lines). (For interpretation of the references to colour in this figure legend, the reader is referred to the web version of this article.)

severity of all but one events can be deduced from other geological constraints.

We underline that the model in Fig. 1, which is based on several assumptions and simplifications, is not meant as a contribution to the debate on damage accumulation and annealing kinetics modelling (Geisler et al., 2001; Geisler, 2002; Ginster et al., 2019; Härtel et al., 2024), but rather as a routine tool to improve geologic interpretations through integration of LA-ICP-MS and Raman analyses. In fact, in our Fig. 1, annealing is invariably modeled to occur in a fixed timeframe of 1 Ma. This implies that, for a given annealing severity, actinide-rich zircons accumulating damage faster are modeled to experience a bigger absolute recovery of α-damage than actinide-poor zircons accumulating damage more slowly. Additionally, young zircon grains characterized by slow damage accumulation (i.e. with little U and Th) are characterized through time by a slow RD_α evolution, which translates into small variations in Raman bandwidths, and are thus prone to larger analytical errors and uncertainties (Fig. 1b vs Fig. 1d).

3. Geological setting and sampling strategy

We applied our conceptual model to the Adamello batholith (Fig. 2), the largest composite intrusive body of the Alps covering an area of ~670 km^2 at the intersection between the Insubric and Giudicarie faults (Callegari and Brack, 2002; Castellarin et al., 2006; Schaltegger et al., 2019). The Adamello batholith is classically divided into five major units intruded between 44 and 29 Ma, showing a younging trend towards the north: Corno Alto-Sostino, Re di Castello, Adamello, Avio-Val di Genova and Presanella (Fig. 2; Del Moro et al., 1983; Mayer et al., 2003; Ji et al., 2019; Schaltegger et al., 2019; Mosconi et al., 2024). The predominant rock types are tonalite and granodiorite, with minor gabbro and diorite emplaced along the margins of the intrusive bodies (Villa, 1983; Callegari and Brack, 2002; Brack. et al., 2008). We focus our analysis on the

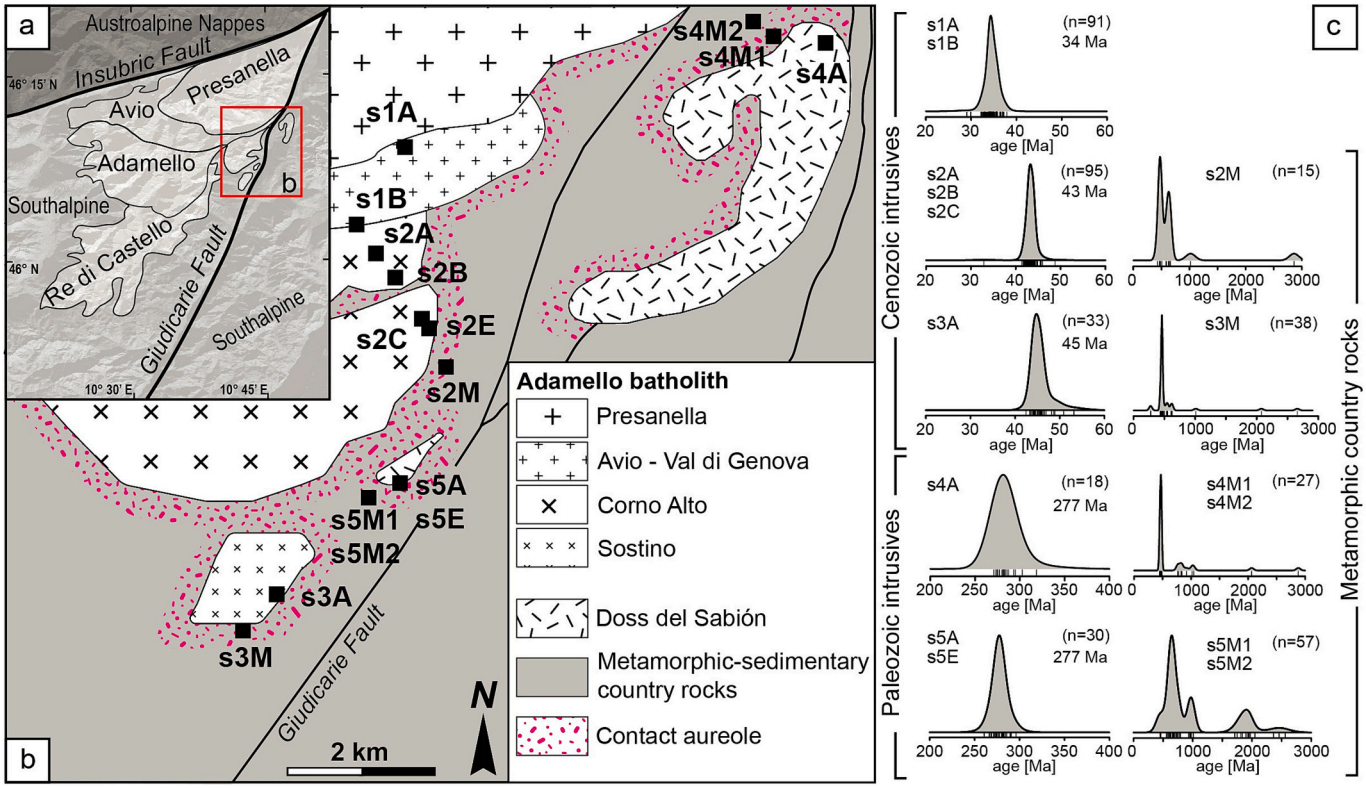

Fig. 2. Simplified geological map of the study area (a), sampling locations (b) and U-Pb ages (c). Kernel density estimates of sampled intrusives in (c) do not include inherited cores.

eastern margin of the batholith, within a study area that includes Eocene-Oligocene plutons (Sostino, Corno Alto and Avio-Val di Genova), Permian intrusives (Doss del Sabión, Borsi et al., 1966), contact aureole and pre-Permian metasedimentary country rocks (Rendena schists) (Fig. 2).

Eighteen bedrock samples (Table 1) were collected along a traverse that spans the contact between plutons of different age and their country rocks within the contact aureole (Fig. 2). They include: two samples of tonalite from the Avio-Val di Genova pluton (s1A and s1B); three samples of granodiorite (s2A, B, C) and a mafic enclave (s2E) from the Corno Alto pluton, and the adjacent schists (s2M); one sample of granodiorite from the Sostino pluton (s3A) and the adjacent basement paragneiss (s3MA) and gneiss (s3MB); one sample of the Doss del Sabión leucogranite east of the Giudicarie Fault (s4A) and the adjacent schists (s4M1 and s4M2B) and gneiss (s4M2A); and one sample of leucogranite (s5A) and a mafic enclave (s5E) from a Permian satellite of the Doss del Sabión west of the Giudicarie Fault and the adjacent schists (s5M1 and s5M2).

Table 1
Sample location (decimal degrees - WGS 84) and lithology.

Sample	Lab code	Latitude	Longitude	Lithology
s1A	*MaSS-7*	46.173891	10.746578	Avio-Val di Genova tonalite
s1B	*MaSS-2*	46.162025	10.736911	Avio-Val di Genova tonalite
s2A	*MaSS-3*	46.158276	10.739682	Corno Alto granodiorite
s2B	*MaSS-4*	46.153794	10.743911	Corno Alto granodiorite
s2C	*MaSS-1*	46.145694	10.748583	Corno Alto granodiorite
s2E	*MaSS-5*	46.144587	10.748381	mafic enclave in Corno Alto granodiorite
s2M	*MaSS-6*	46.138631	10.752152	Rendena schists – Corno Alto country rock
s3A	*MaSS-17*	46.098878	10.727945	Sostino granodiorite
s3M	*MaSS-21A, B*	46.094644	10.721999	Paragneiss (A); gneiss (B)
s4A	*MaSS-8*	46.195557	10.813518	Doss del Sabión leucogranite (east of Giudicarie) Fault)
s4M1	*MaSS-9*	46.196526	10.803241	Rendena schists
s4M2	*MaSS-22A, B*	46.195781	10.801036	Gneiss (A); Schist (B)
s5A	*MaSS-13*	46.118377	10.744003	Doss del Sabión leucogranite (west of Giudicarie) Fault)
s5E	*MaSS-14*	46.11837	10.74402	Country rock enclave
s5M1	*MaSS-15*	46.116258	10.73997	Rendena schists
s5M2	*MaSS-16*	46.116119	10.73987	Rendena schists

4. Analytical methods

An aliquot (2 to 5 kg) of each rock sample was crushed in the laboratories of the University of Milano-Bicocca, using a jaw crusher to obtain <500 μm particles. After dry sieving, zircon grains were concentrated from the 500–250 and 250–125 μm size fraction using standard techniques including hydrodynamic (Gemini shaking table), gravimetric (Na-polytungstate, $\rho = 2.90$ g/cm^3; diiodomethane, $\rho = 3.32$ g/cm^3) and magnetic (isodynamic Frantz magnetic separator at 1.2 A) separation (Malusà and Fitzgerald, 2019). Inclusion-free zircon crystals with no cracks were selected and handpicked under a binocular microscope, with approximately 100 grains per sample being mounted in epoxy resin, splitting each size fraction in two mounts (large and small crystals) to facilitate homogenous polishing. Mounts were polished to expose zircon internal sections and obtain cathodoluminescence images, along with reflected and transmitted-light microscope images, to identify the internal structure and the location spot for laser ablation and Raman analysis.

Raman analysis was conducted at the Provenance Center of the University of Milano-Bicocca, by performing point analyses on previously identified spots on individual zircon crystals. We used a Renishaw® InVia™ Qontor™ spectrometer equipped with a solid-state laser (Nd:YAG) emitting at a wavelength of 532 nm, with an output power of 100 mW and grating of 1800 lines/mm. Analyses were performed at a magnification of 50× with long-working distance objective.

For each analytical point, the sample was exposed focusing the laser (50% laser energy) for 30 cycles of 1 s each. Peak positions and full widths at half maximum (Γ) were determined in Origin™ software using a pseudo-Voigt peak function, and corrected for spectral broadening using the formula proposed by Váczi (2014), using a spectrometer bandpass of 3.7 cm^{-1}. Reproducibility was estimated by repeated measures on both crystalline and metamict zircons and was estimated to be ~7%.

After Raman analysis, LA-ICP-MS U-Pb analyses were conducted at the Laboratory for Accelerators and Applied Superconductivity - LASA (University of Milano), using a spot size of 25 μm, a repetition rate of 10 Hz, a fluence of 2.99 J/cm^2, and a helium gas carrier flux of 0.5 L/min on the same crystals/spots previously analyzed with Raman microprobe. We used the natural zircon 91500 as reference material, the Plešovice zircon as quality control, and the external glass standards NIST610 and NIST612 as reference materials to quantify element compositions. Raw data review, calculation, and analysis of the isotopic ratios were carried out using Glitter and Isoplot software (Ludwig, 2003; Vermeesch, 2018) to obtain crystallization age and U, Th and Pb concentrations. Ages are calculated from LA-ICP-MS ratios as "concordia" ages (Ludwig, 1998) and concordant ages are selected by applying a concordia distance filter of −2/+7 (Vermeesch, 2021).

5. Results

5.1. Zircon U-Pb ages

Analyzed zircon grains from the Adamello batholith show weighted-mean U-Pb ages ranging from 45.28 ± 0.52 Ma (s3A) to 34.45 ± 0.23 Ma (s1A-B) (Fig. 2c), with the Corno Alto pluton (s2A-B-C) yielding ages of 43.15 ± 0.15 Ma. U-Pb ages from the Doss del Sabión pluton range from 277.16 ± 1.4 Ma (s5A, E) to 277.2 ± 2.7 Ma (s4A). The few older cores detected in zircon grains from the Corno Alto and Avio–Val di Genova plutons mostly yield Proterozoic concordant ages. Zircons grains in the pre-Permian country rocks are characterized by multiple peaks reflecting sedimentary protolith provenance, the most prominent one at ~500 Ma and associated with minor peaks at 1.0 and 2.8 Ga (Fig. 2c).

5.2. U and Th concentrations

Zircon grains characterized by both LA-ICP-MS and Raman analyses show variable U and Th concentrations among plutons (see Supplementary material). The concentration of actinides, expressed here as effective Uranium (eU = 1.05 U + 0.24 Th) (Härtel et al., 2021a), is generally higher in plutonic rocks from the Cenozoic Adamello Batholith than from Paleozoic plutons. The eU is even lower in the surrounding country rocks (Fig. 3). The only exception is represented by zircon grains from the Avio-Val di Genova samples (s1A-s1B), which are comparable with those from the Doss del Sabión pluton (s4A and s5A). The Avio-Val di Genova samples (s1B and s1A) host zircon grains with eU ranging from ~132 to 2362 μg/g. The Corno Alto samples (s2A, B, C) yield ~204–9258 μg/g eU. The Sostino sample (s3A) yields ~184–4051 μg/g eU. The Doss del Sabión sample collected east of the Giudicarie Fault (s4A) hosts zircon grains yielding ~221–1164 μg/g eU, whereas zircon grains from the samples collected west of the Giudicarie Fault (s5A, s5E) yield 182–2443 μg/g eU. Country rock samples yield zircon grains roughly within the same range of eU content as the Avio-Val di Genova samples (Fig. 3).

5.3. Raman data screening

Before applying the simplified model described in Sect. 2 to our dataset, Raman data must be screened to ensure consistency. RD_α values are expected to be equal to N_α in case of no annealing after crystallization, or lower than N_α in case of annealing (Fig. 1b,d). Zircon crystals from country rock samples around the Sostino and Doss del Sabión

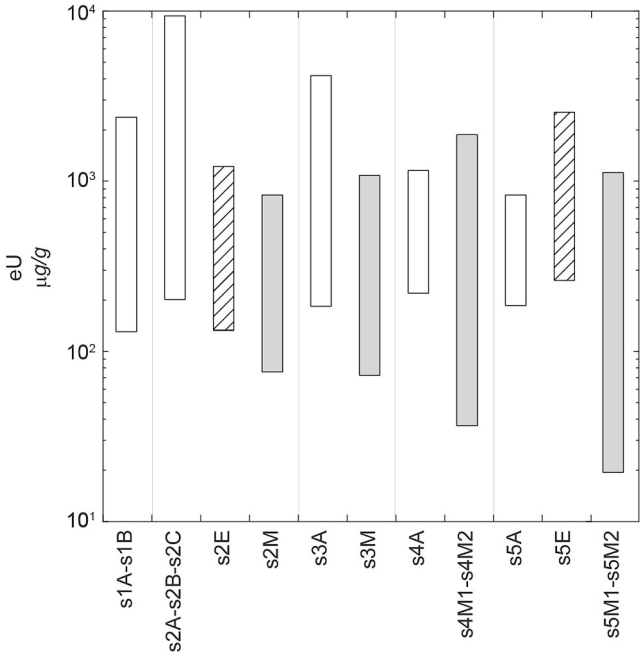

Fig. 3. Effective Uranium (eU) variability in the analyzed zircon grains from the Adamello area samples (white = intrusives; grey = country rocks; hatched = enclaves). Values for magmatic rock samples refer to zircon rims.

plutons (s3M, s4M1, s4M2, s5M1, s5M2) invariably show $RD_\alpha < N_\alpha$, which demonstrates annealing after crystallization. Zircon crystals from the Corno Alto pluton (s2A, s2B, s2C) yield $RD_\alpha \leq N_\alpha$ values, whereas most zircon grains from the Avio-Val di Genova pluton (s1A, s1B) show unrealistic $RD_\alpha > N_\alpha$ average values. In the $RD_{\nu3\alpha}/N_\alpha$ vs. N_α plot of Fig. 4, all samples show similar trends: ratios calculated for low defect densities ($N_\alpha < 10^{17}$ *α-events* g^{-1}) are >1, and progressively decrease towards a flat, nearly constant ratio value ≤1 for higher defect densities ($N_\alpha \geq 10^{17}$ *α-events* g^{-1}), i.e., moving from the left to the right in the diagram of

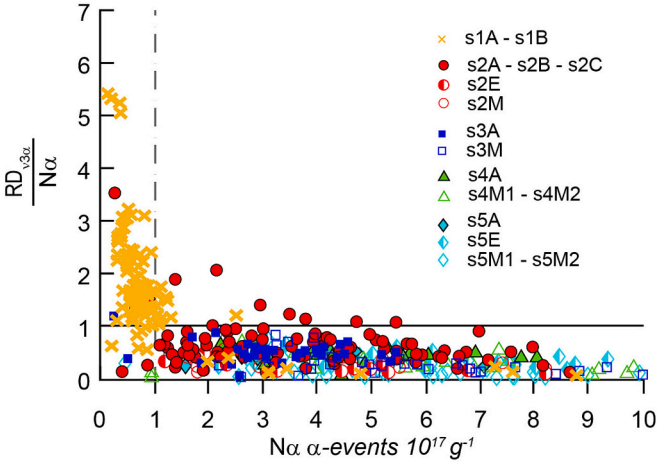

Fig. 4. Defect density estimated by Raman spectroscopy on the ν_3 band ($RD_{\nu3\alpha}$) vs. maximum expected defect density (N_α). $RD_{\nu3\alpha}$ represents the "real" damage accumulated within the zircon grain during its geological history and is expected to be equal (in case of no annealing) or lower (if annealing took place) than N_α (i.e. the α-damage calculated from actinide concentration and age, see Sect.1). Most zircon grains from the Eocene-Oligocene Adamello plutons show values higher than Permian plutons and Paleozoic country rocks. Low-actinide and/or young zircons ($N_\alpha < 10^{17}$ α-events g^{-1}), show unrealistic ratios $RD_{\nu3\alpha}/N_\alpha > 1$ which are considered as an effect of measurement errors when analytical resolution is unable to capture small variations in damage accumulation.

Fig. 4. The number of zircon grains with $N_\alpha < 10^{17}$ *α-events* g^{-1} is higher in samples from the Avio-Val di Genova pluton (s1A and s1B) due to low concentration of actinides and young crystallization age. These unexpected ratios >1 may be ascribed to insufficient resolution of the Raman setup to capture the small variations in Raman bands linked to low damages, or by uncertainties in the linear relationships between Raman band widths and α-damage used to calculate RD_α. Such relationships may not be linear especially for small N_α, see for instance the relationships proposed by Palenik et al. (2003) and Váczi and Nasdala (2017) for the ν_3 band. To circumvent this problem, all zircon crystals with $N_\alpha < 10^{17}$ *α-events* g^{-1} were filtered out and discarded from further analysis. We did not apply the screening procedure described by Härtel et al. (2022) because, using a green laser emission (532 *nm*), photoluminescence could be expected in the spectral region close to the ν_2 band (Lenz and Nasdala, 2015; Anderson et al., 2020). As the ER band is located in a different spectral region, it is not influenced by such photoluminescence effect.

6. Model application and validation

We applied the approach described in Sect. 2 to the zircon grains from the Adamello area. We considered both zircon cores and zircon rims. Results are shown in Fig. 5 and are discussed below.

6.1. Avio–Val di Genova pluton

Zircon rims from the Avio-Val di Genova pluton (samples s1A and s1B) generally show $RD_{ER\alpha}/N_\alpha \sim 1.2$, indicating no annealing (Fig. 5). The crystallization of the Avio-Val di Genova was followed by the emplacement of the Presanella pluton, which occurred only 2 Ma after (Ji et al., 2019, and references therein). However, the short time elapsed between the two events implies that our simplified model cannot discriminate between the two events, given the little damage accumulated by actinide-poor zircon grains in such a short timeframe. Inherited cores, instead, show $RD_{ER\alpha}/N_\alpha \sim 0.18$, clearly pointing to severe annealing. The age of the complete annealing event is scattered from 50 to over 200 Ma. These inherited cores were included in the magma chamber at ~34 Ma, at a much later stage of the geologic evolution, as revealed by the crystallization age of analyzed zircon rims. Therefore, the most probable age of the thermal event responsible for annealing is ~34 Ma, corresponding to the intrusion age of the magma hosting the overgrown cores. As the age of the thermal event is younger than the threshold of the calculated maximum age of total annealing, annealing was necessarily incomplete. Modelling suggests that annealing at 34 Ma obliterated ~90% of the previously accumulated damage (Fig. 5a).

6.2. Corno Alto pluton

Zircon rims from the Corno Alto pluton (s2A, s2B, s2C) generally show $RD_{ER\alpha}/N_\alpha \sim 0.75$, indicating that some annealing took place after their crystallization at ~43 Ma. Application of our simplified model suggests generalized annealing occurring at ~34 Ma, corresponding to the crystallization age of the nearby Avio-Val di Genova pluton.

Looking at these samples in more detail, zircon grains roughly show

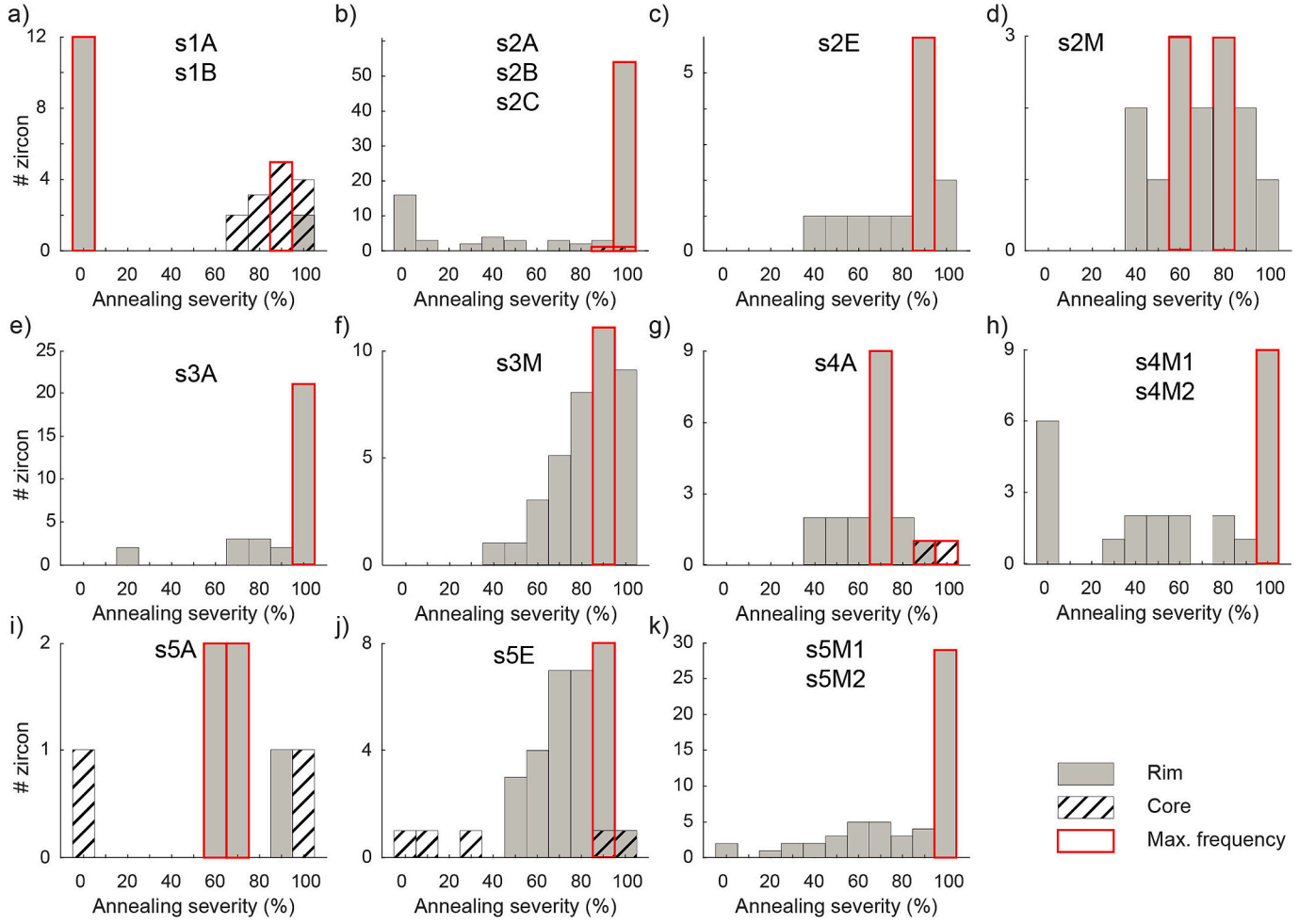

Fig. 5. Annealing severity based on the simplified model of Fig. 1. For the Doss del Sabión country rocks (s4M1, s4M2, s5M1, s5M2) only the annealing severity for the Permian event is shown.

two distinct behaviors in terms of annealing severity: more than a half of them are fully annealed, whereas about a fifth of them preserve most of the damage accumulated since crystallization (Fig. 5b). Among the latter, 17 out 19 belong to the sample s2C, which has been collected farthest away from the Avio-Val di Genova pluton (see Fig. 2b). These zircon grains are also invariably smaller and characterized by lower concentrations of actinides. Two inherited cores from sample s2C show low $RD_{ER\alpha}/N_\alpha$ (~ 0.1) and, irrespective of their previous annealing history, they show damage values ($RD_{ER\alpha}$) consistent with severe annealing at ~34 Ma.

Zircon grains from the mafic enclave in the Corno Alto pluton (s2E), collected close to sample s2C, show $RD_{ER\alpha}/N_\alpha$ ~ 0.32 that agree with almost complete annealing (~ 90%) during the crystallization of Corno Alto zircons (~ 43 Ma) (Fig. 5c). Zircons from the country rock surrounding the Corno Alto pluton (sample s2M) show $RD_{ER\alpha}/N_\alpha$ ~ 0.37, also indicating annealing. These zircons could be either completely annealed at ~220 Ma or, if the crystallization age of the Corno Alto is considered (43 Ma), annealing severity is calculated as 60–80% (Fig. 5d).

6.3. Sostino pluton

Zircon grains from the Sostino pluton (s3A) show $RD_{ER\alpha}/N_\alpha$ values ~0.67 that reveal annealing (Fig. 5e). Our simplified model is consistent with complete annealing caused by the emplacement of the Corno Alto pluton (Fig. 6a). However, the limited time difference between the crystallization age of the Sostino (45 Ma) and Corno Alto (43 Ma) plutons, and the little damage accumulated in those 2 Ma, dramatically lower the resolution of the modelling. Better results are achieved when modelling a younger annealing at ~34 Ma, corresponding to the emplacement of the Avio-Val di Genova pluton, because of the longer time span available for damage accumulation. This might appear in contrast with the moderate annealing of sample s2C, located closer to the Avio-Val di Genova pluton, but the mismatch could be explained with the largely unknown three-dimensional configuration of the plutonic bodies at the time of intrusion. A third alternative interpretation may be provided by two subsequent annealing events at 43 and 34 Ma.

Country rock zircon grains beside the Sostino pluton (s3M) show

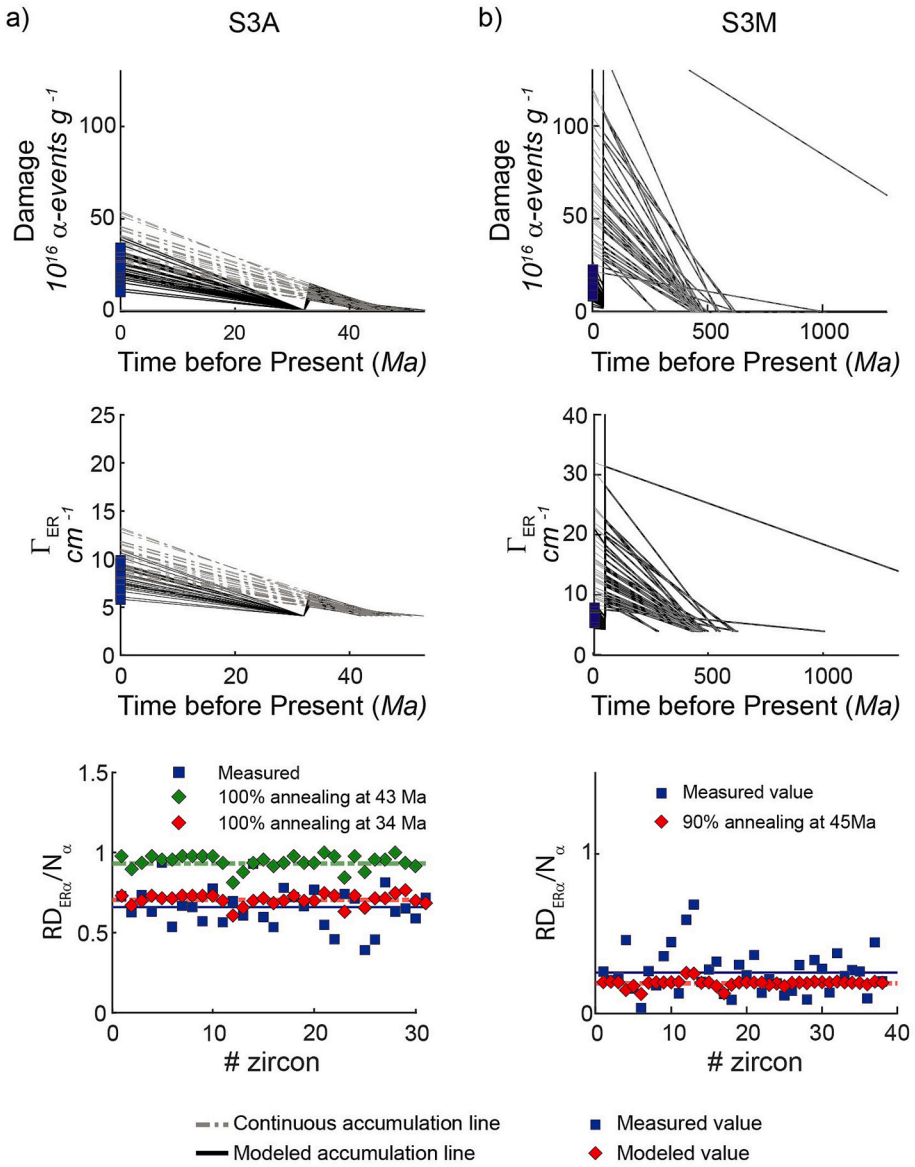

Fig. 6. Modeled evolution of damage accumulation for zircon grains from the Sostino pluton s3A (a) and adjacent country rock s3M (b). Top row: modeled evolution of damage accumulation; Central row: modeled evolution of Γ_{ER}; bottom row: Measured and modeled $RD_{ER\alpha}/N_\alpha$ ratios. For the Sostino pluton (a), top and central rows show the modeled evolution for annealing at 34 Ma, while the bottom row shows the $RD_{ER\alpha}/N_\alpha$ ratios for annealing at both 43 and 34 Ma.

$RD_{ER\alpha}/N_\alpha$ ~ 0.25. Total annealing would have taken place at ~110 or 480 Ma, which is geologically meaningless as no thermal event is known from the geological record of the area, whereas annealing at ~45 Ma due to the intrusion of the Sostino pluton would have a severity of ~90% (Figs. 5f, 6b).

6.4. Doss del Sabión pluton

Zircon rims from sample s4A, collected from the Permian Doss del Sabión pluton to the east of the Giudicarie Fault (Fig. 2b), reveal average $RD_{ER\alpha}/N_\alpha$ ~ 0.40, compatible with annealing at 34 Ma and a modeled annealing severity of 70% (Fig. 5g, Table 2). Total annealing would have instead taken place at ~120 Ma, which is geologically meaningless. The two zircon cores analyzed in sample s4A record nearly complete annealing at the time of Doss del Sabión crystallization, followed by 70% annealing at 34 Ma as recorded by the zircon rims.

Modelling of nearby country rock zircon grains (s4M1 and s4M2) reveals a thermal evolution similar to the s4A zircon core, and therefore affected by both the Doss del Sabión and Avio-Val di Genova intrusions. Most of the zircon grains from sample s4M1, located closer to the Doss del Sabión pluton, show higher degree of annealing than zircon grains from sample s4M2, located at a greater distance from the pluton. Annealing severity positively correlates with actinide content (Fig. 5h).

Zircon rims from sample s5A, collected from the Doss del Sabión pluton to the west of the Giudicarie Fault, show average $RD_{ER\alpha}/N_\alpha$ ~ 0.40 and are compatible with complete annealing between 60 and 100 Ma, again geologically meaningless. If we consider the intrusion of the closest pluton (43 Ma, Corno Alto granodiorite) as the most probable cause for annealing, the severity is estimated around 60–70%. Zircon core data, when the same degree of annealing as the zircon rims is imposed for the emplacement of the Corno Alto pluton, indicate contrasting annealing during the Doss del Sabión crystallization (~ 280 Ma) ranging from 0 to 100%. It must be noted that annealing severity positively correlates with one order of magnitude variation in actinide concentration, and the low degree of Permian annealing in some zircon cores may thus likely be due to increased analytical errors (see Sect. 2). Zircon grains rims from the enclave s5E yield ER_α/N_α ~ 0.36 and fit with ~70–90% annealing at 43 Ma, similar to what has been modeled for the Doss del Sabión plutonic rocks exposed either to the west or to the east of the Giudicarie Fault. Zircon cores point towards annealing as testified to by ER_α/N_α values ~0.23. Low-actinide concentrations (200–600 μg/g eU) provide contrasting results with variable degree of annealing linked to the Dos del Sabión emplacement, when the same degree of annealing at 43 Ma suffered by zircon rims is imposed. Zircon annealing data from the surrounding country rocks (s5M1 and s5M2), characterized by ER_α/N_α ~ 0.17, fit with complete annealing at 280 Ma followed by partial (~ 70%) annealing at 43 Ma, as deduced from sample s5A.

Table 2
Annealing severity in zircon grains from the main plutonic bodies of the Adamello area and surrounding country rocks.

Unit	Sample	Annealing event	
		Adamello (34–45 Ma)	Doss del Sabión (280 Ma)
Avio Val di Genova	s1A-s1B rim	0%	–
	s1A-s1B core	90%	–
Corno Alto	s2A-s2B-s2C rim	100%	–
	s2A-s2B-s2C core	90–100%	–
	s2E	90%	–
	s2M	60–80%	–
Sostino	s3A	100%	–
	s3M	90%	–
	s4A rim	70%	–
	s4A core	70%	90–100%
	s4M1-s4M2	70%	100%
Doss de Sabión	s5A rim	60–70%	–
	s5A core	70%	0, 100%
	s5E rim	70–90%	–
	s5E core	80%	0, 100%
	s5M1-s5M2	70%	100%

6.5. Geological validation of the simplified annealing model

Our results provide insights on the complex thermal interactions among different magmatic bodies and associated country rocks exposed along the eastern margin of the composite Adamello batholith, and on the viability of the simplified model proposed in Sect. 2. The overall robustness of our approach is supported by the following observations:

(i) All the Adamello zircon rims invariably show a complex annealing history whereby the older plutons have experienced annealing induced by the intrusion and crystallization of progressively younger bodies, with the only exception of the young Avio-Val di Genova pluton.
(ii) Inherited zircon cores in all the Adamello samples invariably record damage accumulation only starting from the age of rim crystallization, whereas all previous damage had been annealed during incorporation in the Eocene-Oligocene magma.
(iii) Zircon grains from the Permian Doss del Sabión pluton show the same annealing effects as zircons from the Cenozoic Adamello batholith, but with less relative annealing due to a higher level of damage accumulated between Permian crystallization and Cenozoic annealing.
(iv) Severity of annealing in country rock zircons roughly correlates with distance from the closest plutons (e.g., s3M, being collected close to the Sostino body, shows annealing ~90%, whereas samples s2M and s5M1 and s5M2, collected at some distance from the Corno Alto and Doss de Sabión plutons, show lower annealing severities).

7. Detrital test and application to provenance studies

Our ability to discriminate different detrital zircon-grain populations in a dataset is crucial in provenance studies. When zircon U-Pb data cluster around a limited number of ages that are widespread over the potential source areas, the possibility of further distinguishing grain-age populations based on their post-crystallization history may help increase the resolution of provenance estimates. To test if our bedrock approach can be exported to the analysis of detrital systems, all zircon crystals described in the previous sections have been lumped in a single dataset to simulate a synthetic detrital zircon sample of unknown provenance (Fig. 7a). As the main difference between bedrock and detrital-grain populations is a common thermal history for all the crystals of the former, and the a-priori unknown provenance of zircon grains of the latter, most of the assumptions based on geological knowledge that have been made in the previous sections, for example the age of annealing, are no longer viable and additional assumptions and generalizations are required. This implies that the resolution of the results will be lowered by the lack of knowledge on the thermal evolution of the source rocks.

In our synthetic detrital sample, the U-Pb age distribution reveals three well defined populations with a bimodal peak at ~34–43 Ma, two unimodal peaks at ~278 and ~ 476 Ma, and other minor older peaks up to 2.5 Ga (Fig. 7a). For each zircon grain, we estimate the age of total annealing as the age from which damage started to be accumulated in the crystalline structure of the zircon grain (i.e. ages that allow $RD_{ER\alpha}/D_\alpha$ values within the 0.9–1.1 range). If the estimated total annealing age is ±10 Ma with respect to the U-Pb age of the crystal, we consider the zircon grain to be unaffected by annealing after crystallization. In our dataset, 135 grains out of 356 can be considered to have completely retained damage since their crystallization. Most of them belong to the youngest U-Pb age population at ~34–43 Ma, where they represent 99% of the peak. Only a few of them belong to the ~278 Ma population,

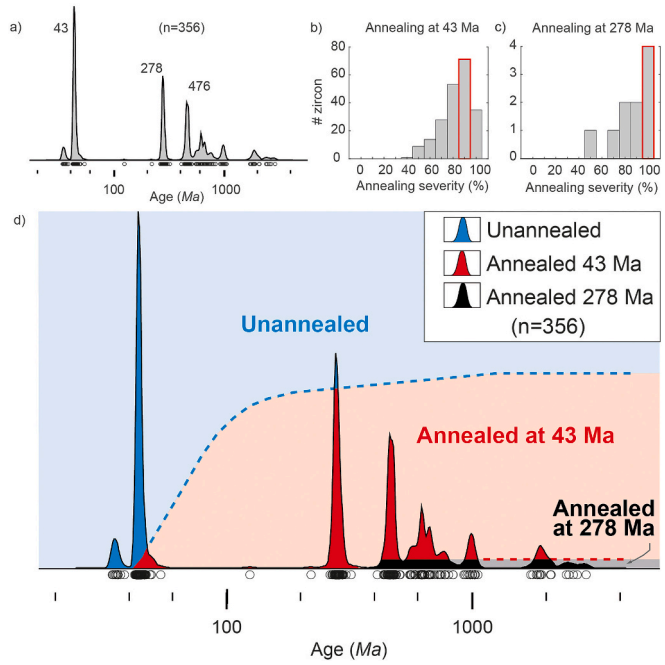

Fig. 7. a) Age spectrum simulating a detrital sample derived from the erosion of the area depicted in Fig. 2. Note that bedrock sampling has preferentially targeted plutonic rocks, and Adamello ages are thus overrepresented. On the other hand, it should be noted that zircon fertility in plutonic rocks is higher than in meta-sedimentary country rocks; b) Modeled evolution and severity of annealing for "detrital" zircon affected by annealing at 43 Ma; c) Modeled evolution and severity of annealing for "detrital" zircon affected by annealing at 280 Ma; d) Improved zircon provenance discrimination by combined U-Pb and Raman analyses. The three grain age populations can be further subdivided according to their annealing history: the youngest population is characterized by no annealing, whereas all oldest grains and almost all grains of the 278 Ma age peak show annealing mostly during the 43 Ma event.

representing 7% of the peak, whereas none of them belong to the older populations. This implies that 221 grains, i.e., 62% of the zircon grains included in our synthetic detrital dataset, show $RD_{ER\alpha}/D_{\alpha} < 1$ and underwent annealing since their crystallization.

Without any a-priori knowledge on the evolution of the source areas, as generally expected in detrital studies, we can use the age of the main populations found in the detrital U-Pb age spectra (i.e., ~ 43 and ~ 278 Ma) as the age of potential annealing for these 221 zircon grains. These ages are in fact expected to reflect major magmatic/metamorphic events in the source area. To determine their age of annealing, zircon grains have been split into two groups based on their estimated complete annealing age: those compatible with an estimated complete annealing age equal or older than 278 ± 10 Ma are considered to be affected by a Paleozoic magmatic event at ~278 Ma (~ 10 grains), while the others are considered to be affected by an Eocene magmatic event at ~43 Ma (~ 211 grains). These zircon grains are thus classified as 38% as being not annealed, 59% as annealed ~43 Ma (independently of their crystallization age) and 3% as annealed ~278 Ma. These percentages reflect the present-day distribution of different rock types (i.e., Cenozoic vs Paleozoic intrusives) in the geological map of Fig. 2, and the original sampling strategy that targeted mostly the Cenozoic plutonic rocks.

In more detail, zircon grains affected by the ~278 Ma thermal event are supportive of almost complete annealing (Fig. 7b), in general agreement with the results obtained with bedrock data (Table 2) although in the detrital test we hypothesize a single annealing event. As revealed by their U-Pb age, they derive from country rock samples testifying to the general thermal overprint experienced by these rocks in Permian times. Zircons affected by the ~43 Ma event show annealing severity around 90% (Fig. 7c). They chiefly derive from the Doss del Sabión pluton as well as from the zircon cores of the Adamello pluton and the surrounding country rocks.

These results demonstrate that the application of our model complementing detrital U-Pb ages with Raman spectroscopy allows increasing the resolution of provenance discrimination, providing a level of information approaching the evolution inferred from bedrock data. In fact, the three main U-Pb age populations identified by LA-ICP-MS analyses can be further characterized in terms of geological evolution and annealing history: (i) zircon grains crystallized around ~43 Ma are largely unannealed and derive from the Cenozoic plutons; (ii) zircon grains yielding U-Pb ages around ~278 Ma mostly show annealing at ~43 Ma (~ 93% of the 278 Ma population), although some grains (~ 7%) are not affected by annealing; (iii) zircon grains characterized by older crystallization ages (~ 400 Ma and older) have invariably been annealed by younger thermal events at ~278 Ma (~ 6% of the oldest populations) and ~ 43 Ma (~ 94%).

In summary, with only the information provided by U-Pb ages and annealing history derived from Raman analyses, zircon grain provenance can be interpreted as characterized by (Fig. 8):

(i) A main source crystallized at ~43 Ma that experienced continuous damage accumulation, contributing for ~37% of the zircon grain population. This source includes the analyzed zircon rims from the Avio-Val di Genova, Corno Alto and Sostino plutons. The annealing effects produced by younger magmatic pulses on older Cenozoic plutons, as discussed in Sect. 6, are not detected here as we lack any a-priori geological knowledge, and because the intrusion age differences are small.

(ii) A source crystallized at ~278 Ma, contributing fewer grains (~ 19%) and mostly affected by the 43 Ma annealing event (~ 18% of the entire population). This source mostly includes zircon rims from the Doss del Sabión pluton and the surrounding country rocks that were thermally affected by the emplacement of plutonic rocks at ~43 Ma, and a few zircons (~ 1% of the total number of analyzed zircon grains) from the Doss del Sabión intrusive east of the Giudicarie Fault and country rocks that escaped annealing.

(iii) Older zircons (~ 44% of the entire population) that invariably show annealing at ~43 and ~ 280 Ma. Almost all these zircons (94% of this group and 41% of the entire population) show annealing at ~43 Ma, testifying that this is the age of the main thermal event in the source area. Zircons with U-Pb age signature >400 Ma are inherited cores within plutons and country rocks.

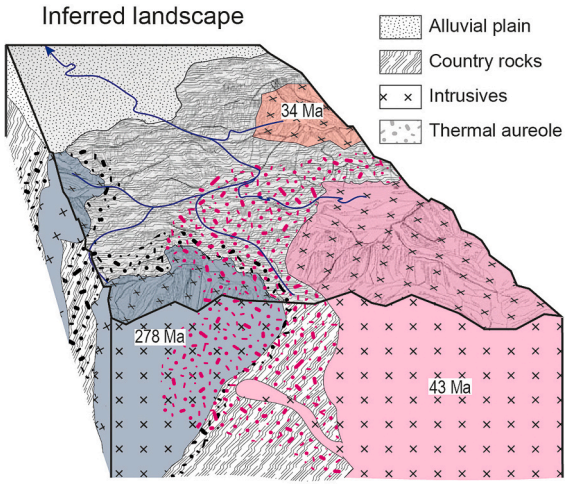

Fig. 8. Hypothetical landscape inferred from combined zircon U-Pb and Raman data in the lack of a-priori geological constraints.

8. Conclusions

Our study presents a simple conceptual model to improve geologic interpretations of bedrock and detrital zircon datasets through integration of U-Pb and Raman analysis. It compares the α-damage expected from U-Pb data and the actual damage resulting from damage accumulation and (partial) annealing as measured by Raman spectroscopy. The model was tested in the Cenozoic Adamello composite batholith, a natural laboratory in the European Alps where the progressive emplacement of successive, radiometrically dated magmatic bodies has thermally affected both the metamorphic country rocks and the previously emplaced igneous rocks under well-constrained geological conditions. The robustness of our approach is demonstrated by the following empirical results: (i) zircon rims from the Adamello batholith invariably show a complex, but fully predictable annealing history after crystallization, as induced by subsequent intrusion of younger plutonic bodies; (ii) zircon cores record damage accumulation invariably starting from the age of rim crystallization; (iii) the severity of annealing in country rock zircons correlates with distance from the nearby plutons.

Our results on bedrock zircon were then exported to a synthetic detrital zircon population to test how the impact of reheating can be detected in detrital zircon datasets. We found that the application of our model allows increasing the resolution of provenance discrimination to a level approaching the information inferred from bedrock data. This suggests that an approach to detrital zircon geochronology complementing detrital U-Pb ages with Raman spectroscopy could be routinely used in other study areas to improve sediment provenance analysis in the lack of independent geological constraints, opening new venues for provenance studies.

CRediT authorship contribution statement

Alberto Resentini: Writing – original draft, Visualization, Validation, Supervision, Resources, Methodology, Investigation, Formal analysis, Data curation, Conceptualization. **Marco G. Malusà:** Writing – original draft, Visualization, Resources, Methodology, Investigation, Conceptualization. **Silvia Favaro:** Writing – original draft, Visualization, Investigation, Formal analysis, Data curation. **Michele Longhi:** Investigation, Formal analysis. **Massimo Tiepolo:** Writing – review & editing, Supervision, Resources, Methodology. **Igor M. Villa:** Writing – review & editing, Conceptualization. **Stefano Zanchetta:** Writing – review & editing, Supervision, Resources, Project administration, Investigation, Funding acquisition, Conceptualization.

Declaration of competing interest

The authors declare that they have no known competing financial interests or personal relationships that could have appeared to influence the work reported in this paper.

Acknowledgments

This article is an outcome of Project MIUR – Dipartimenti di Eccellenza 2018–2022. The revised manuscript benefited from insightful comments provided by Birk Härtel and an anonymous reviewer.

Appendix A. Supplementary data

Supplementary data to this article can be found online at https://doi.org/10.1016/j.chemgeo.2026.123486.

Data availability

Data will be made available on request.

References

Anderson, A.J., Hanchar, J.M., Hodges, K.V., van Soest, M.C., 2020. Mapping radiation damage zoning in zircon using Raman spectroscopy: Implications for zircon chronology. Chem. Geol. 538, 119494. https://doi.org/10.1016/j.chemgeo.2020.119494.

Borsi, S., Ferrara, G., Tongiorgi, E., 1966. Rb/Sr and K/Ar ages of intrusive rocks of Adamello and M. Sabion (Trentino, Italy). Earth Planet. Sci. Lett. 1 (2), 55–57. https://doi.org/10.1016/0012-821X(66)90105-1.

Brack., P., Baroni, C., Carton, A., Pellegrini, G.B., Nardin, M., Pennacchioni, G., 2008. Note Illustrative della Carta geologica d'Italia alla scala 1:50.000, F. 058 Monte Adamello. Servizio Geologico d'Italia – ISPRA, 144 pp.

Callegari, E., Brack, P., 2002. Geological Map of the Tertiary Adamello Batholith (Northern Italy): Explanatory Notes and Legend. Mem. Sci. Geol. 54, 19–49.

Castellarin, A., Vai, G.B., Cantelli, L., 2006. The Alpine evolution of the Southern Alps around the Giudicarie faults: a Late Cretaceous to Early Eocene transfer zone. Tectonophysics 414 (1–4), 203–223. https://doi.org/10.1016/j.tecto.2005.10.019.

Dawson, P., Hargreave, M.M., Wilkinson, G.R., 1971. The vibrational spectrum of zircon (ZrSiO4). J. Phys. C Solid State Phys. 4-2, 240–256. https://doi.org/10.1088/0022-3719/4/2/014.

Del Moro, A., Pardini, G., Quercioli, C., Villa, I.M., Callegari, E., 1983. Rb/Sr and K/Ar chronology of the Adamello granotoids, Southern Alps. Mem. Soc. Geol. Ital. 26, 285–301.

Ewing, R.C., Chakoumakos, B.C., Lumpkin, G.R., Murakami, T., 1987. The metamict state. Mater. Res. Soc. Bull. 12 (4), 58–66. https://doi.org/10.1557/S0883769400067865.

Fan, M., Liu, X., Sun, S., Dong, Y., Ayers, J.C., Santosh, M., 2023. Effect of chemical composition on zircon radiation damage dating: Implications for low-temperature thermochronology. Geosci. Front. 14 (6), 101675. https://doi.org/10.1016/j.gsf.2023.101675.

Geisler, T., 2002. Isothermal annealing of partially metamict zircon: evidence for a three-stage recovery process. Phys. Chem. Miner. 29 (6), 420–429. https://doi.org/10.1007/s00269-002-0249-3.

Geisler, T., Pidgeon, R.T., van Bronswijk, K., Pleysier, R., 2001. Kinetics of thermal recovery and recrystallization of partially metamict zircon – a Raman spectroscopic study. Eur. J. Mineral. 13, 1163–1176. https://doi.org/10.1127/0935-1221/2001/0013-1163.

Ginster, U., Reiners, P.W., Nasdala, L., Chutimun, Chanmuang N., 2019. Annealing kinetics of radiation damage in zircon. Geochim. Cosmochim. Acta 249, 225–246. https://doi.org/10.1016/j.gca.2019.01.033.

Harley, S.L., Kelly, N.M., 2007. Zircon tiny but timely. Elements 3 (1), 13–18. https://doi.org/10.2113/gselements.3.1.13.

Härtel, B., Jonckheere, R., Wauschkuhn, B., Hofmann, M., Frölich, S., Ratschbacher, L., 2021a. Zircon Raman dating: Age equation and calibration. Chem. Geol. 579, 120351. https://doi.org/10.1016/j.chemgeo.2021.120351.

Härtel, B., Jonckheere, R., Wauschkuhn, B., Ratschbacher, L., 2021b. The closure temperature(s) of zircon Raman dating. Geochronology 3, 259–272. https://doi.org/10.5194/gchron-3-259-2021.

Härtel, B., Jonckheere, R., Ratschbacher, L., 2022. Multi-band Raman analysis of radiation damage in zircon for thermochronology: Partial annealing and mixed signals. Geochem. Geophys. Geosyst. 23, e2021GC010182. https://doi.org/10.1029/2021GC010182.

Härtel, B., Enkelmann, E., Jonckheere, R., Ludwig, T., Krause, J., Ratschbacher, L., 2024. In search of lost time: Raman thermochronology of FC-1 zircon. Contrib. Mineral. Petrol. 179, 2. https://doi.org/10.1007/s00410-023-02083-z.

Holland, H.D., Gottfried, D., 1955. The effect of nuclear radiation on the structure of zircon. Acta Crystallogr. 8, 291–300. https://doi.org/10.1107/S0365110X55000947.

Jaffey, A.H., Flynn, K.F., Glendenin, L.E., Bentley, W.C., Essling, A.M., 1971. Precision measurement of the half-lives and specific activities of 235U and 238U. Phys. Rev. C 4, 1889–1906. https://doi.org/10.1103/PhysRevC.4.1889.

Ji, W.Q., Malusà, M.G., Tiepolo, M., Langone, A., Zhao, L., Wu, F.Y., 2019. Synchronous Periadriatic magmatism in the Western and Central Alps in the absence of slab breakoff. Terra Nova 31 (2), 120–128. https://doi.org/10.1111/ter.12377.

Kolesov, B., Geiger, C.A., Armbruster, T., 2001. The dynamic properties of zircon studied by single-crystal X-ray diffraction and Raman spectroscopy. Eur. J. Mineral. 13, 939–948. https://doi.org/10.1127/0935-1221/2001/0013-0939.

Lenz, C., Nasdala, L., 2015. A photoluminescence study of REE3+ emissions in radiation-damaged zircon. Am. Mineral. 100, 1123–1133. https://doi.org/10.2138/am-2015-4894CCBYNCND.

Ludwig, K.R., 1998. On the treatment of concordant uranium-lead ages. Geochim. Cosmochim. Acta 62, 665–676. https://doi.org/10.1016/S0016-7037(98)00059-3.

Ludwig, K.R., 2003. User's Manual for Isoplot 3.00: a Geochronological Toolkit for Microsoft Excel. Berkeley Geochronology Center Special Publication 4, p. 4.

Malusà, M.G., Fitzgerald, P.G. (Eds.), 2019. Fission-Track Thermochronology and its Application to Geology. Springer. https://doi.org/10.1007/978-3-319-89421-8.

Malusà, M.G., Garzanti, E., 2019. The sedimentology of detrital thermochronology. In: Malusà, M.G., Fitzgerald, P. (Eds.), Fission-Track Thermochronology and Its Application to Geology. Springer, pp. 123–143. https://doi.org/10.1007/978-3-319-89421-8_7.

Malusà, M.G., Carter, A., Limoncelli, M., Villa, I.M., Garzanti, E., 2013. Bias in detrital zircon geochronology and thermochronometry. Chem. Geol. 359, 90–107. https://doi.org/10.1016/j.chemgeo.2013.09.016.

Mayer, A., Cortiana, G., Dal Piaz, G., Deloule, E., Pieri, R., Jobstraibizer, P., 2003. U-Pb single zircon ages of the Adamello batholith, Southern Alps. Mem. Sci. Geol. 55, 151–167.

McKanna, A.J., Koran, I., Schoene, B., Ketcham, R.A., 2023. Chemical abrasion: the mechanics of zircon dissolution. Geochronology 5, 127–151. https://doi.org/10.5194/gchron-5-127-2023.

Mosconi, A., Cannaò, E., Farina, M., Malusà, M.G., Zanchetta, S., Tiepolo, M., 2024. The Corno Alto complex (Adamello batholith): a modern analogue of the high Ba/K sanukitoids. Lithos 470, 107522. https://doi.org/10.1016/j.lithos.2024.107522.

Murakami, T., Chakoumakos, B.C., Ewing, R.C., Lumpkin, G.R., Weber, W.J., 1991. Alpha-decay event damage in zircon. Am. Mineral. 76, 1510–1532.

Nasdala, L., Pidgeon, R.T., Wolf, D., Irmer, G., 1998. Metamictization and U-Pb isotopic discordance in single zircons: a combined Raman microprobe and SHRIMP ion probe study. Mineral. Petrol. 62 (1–2), 1–27. https://doi.org/10.1007/BF01173760.

Nasdala, L., Wenzel, M., Vavra, G., Irmer, G., Wenzel, T., Kober, B., 2001. Metamictisation of natural zircon: accumulation versus thermal annealing of radioactivity-induced damage. Contrib. Mineral. Petrol. 141 (2), 125–144. https://doi.org/10.1007/s004100000235.

Palenik, C.S., Nasdala, L., Ewing, R.C., 2003. Radiation damage in zircon. Am. Mineral. 88 (5–6), 770–781. https://doi.org/10.2138/am-2003-5-606.

Pidgeon, R.T., Nasdala, L., Todt, W., 1998. Determination of radiation damage ages on parts of zircon grains by Raman microprobe: implications for annealing history and U-Pb stability. Mineral. Mag. 62A, 1174–1175.

Resentini, A., Andò, S., Garzanti, E., Malusà, M.G., Pastore, G., Vermeesch, P., Chanvry, E., Dall'Asta, M., 2020. Zircon as a provenance tracer: Coupling Raman spectroscopy and UPb geochronology in source-to-sink studies. Chem. Geol. 555, 119828. https://doi.org/10.1016/j.chemgeo.2020.119828.

Schaltegger, U., Nowak, A., Ulianov, A., Fisher, C.M., Gerdes, A., Spikings, R., Whitehouse, M.J., Bindeman, I., Hanchar, J.M., Duff, J., Vervoort, J.D., Sheldrake, T., Caricchi, L., Brack, P., Müntener, O., 2019. Zircon petrochronology and 40Ar/39Ar thermochronology of the Adamello Intrusive Suite, N. Italy: monitoring the growth and decay of an incrementally assembled magmatic system. J. Petrol. 60 (4), 701–722. https://doi.org/10.1093/petrology/egz010.

Schoene, B., Michael, P.E., Samperton, K.M., Brenhin Keller, C., Keller, G., Adatte, T., Khadri, S.F.R., 2019. U-Pb constraints on pulsed eruption of the Deccan Traps across the End-Cretaceous mass extinction. Science 363 (6429), 862–866. https://doi.org/10.1126/science.aau2422.

Su, K., Zhang, S.B., Hanchar, J.M., Li, Z.X., Sun, F.Y., Liang, T., Gao, X.Y., 2023. Quantification of radiation damage in natural and synthetic zircon by Raman spectroscopy: application to low-temperature thermochronology. Acta Geochim. 42, 673–688. https://doi.org/10.1007/s11631-023-00606-w.

Váczi, T., 2014. A new, simple approximation for the deconvolution of instrumental broadening in spectroscopic band profiles. Appl. Spectrosc. 68 (11), 1274–1278. https://doi.org/10.1366/13-07275.

Váczi, T., Nasdala, L., 2017. Electron-beam-induced annealing of natural zircon: a Raman spectroscopic study. Phys. Chem. Miner. 44, 389–401. https://doi.org/10.1007/s00269-016-0866-x.

Velbel, M.A., 1999. Bond strength and the relative weathering rates of simple orthosilicates. Am. J. Sci. 299, 679–696.

Vermeesch, P., 2018. IsoplotR: a free and open toolbox for geochronology. Geosci. Front. 9, 1479–1493. https://doi.org/10.1016/j.gsf.2018.04.001.

Vermeesch, P., 2021. On the treatment of discordant detrital zircon U–Pb data. Geochronology 3, 247–257. https://doi.org/10.5194/gchron-3-247-2021.

Villa, I.M., 1983. $^{40}Ar/^{39}Ar$ chronology of the Adamello gabbros, Southern Alps. Mem. Soc. Geol. Ital. 26, 309–318.

Voice, P.J., Kowalewski, M., Eriksson, K.A., 2011. Quantifying the timing and rate of crustal evolution: global compilation of radiometrically dated detrital zircon grains. J. Geol. 119 (2), 109–126. https://doi.org/10.1086/658295.

Zhang, M., Salje, E.K., Capitani, G.C., Leroux, H., Clark, A.M., Schlüter, J., Ewing, R.C., 2000. Annealing of alpha-decay damage in zircon: a Raman spectroscopic study. J. Phys. Condens. Matter 12 (13), 3131–3148. https://doi.org/10.1088/0953-8984/12/13/321.

Zhang, Y., Li, R., Zhou, G.-Y., Chew, D., Zengh, J.-P., Xiong, Q., Wang, W., 2026. Zircon thermal annealing ages determining late Eocene birth of the first bend of the Yangtze River. Earth Planet. Sci. Lett. 679, 119888. https://doi.org/10.1016/j.epsl.2026.119888.